

## Phase stability and magnetism of Ni<sub>3</sub>Al

Jian-hua Xu

*Department of Physics and Astronomy, Northwestern University, Evanston, Illinois 60208  
and Shanghai Institute of Metallurgy, Academy of Sciences of China, 865 Chang Ning Road, Shanghai 200 050, China*

B. I. Min

*Department of Physics and Astronomy, Northwestern University, Evanston, Illinois 60208  
and Department of Physics, Pohang Institute of Science and Technology, P.O. Box 125, Pohang 680, Korea*

A. J. Freeman

*Department of Physics and Astronomy, Northwestern University, Evanston, Illinois 60208*

T. Oguchi

*Department of Physics and Astronomy, Northwestern University, Evanston, Illinois 60208  
and The National Research Institute for Metals, 2-3-12 Nakameguro, Meguro-ku, Tokyo 153, Japan*

(Received 19 September 1989)

The structural phase stability of Ni<sub>3</sub>Al is investigated for its cubic ( $L_{12}$ ), tetragonal ( $DO_{22}$ ), and hexagonal ( $DO_{19}$ ) crystal structures with use of an all-electron total-energy local-density-functional approach. In agreement with experiment, the (weakly) ferromagnetic  $L_{12}$  structure is found to be the most stable phase. The calculated lattice constant (3.55 Å), the bulk modulus (2.1 Mbar), and the heat of formation (44.8 kcal/mol) are in fairly good agreement with experiment. The second-nearest-neighbor coupling between Ni  $d$  and Ni  $d$  states and the (higher-order) nearest-neighbor coupling between Ni  $d$  and Al  $p$  states may play an important role in accounting for the structural stability of Ni<sub>3</sub>Al. The inclusion of spin-orbit coupling is found to reduce the exchange-energy splitting and magnetic moment by  $\sim 40\%$ .

### I. INTRODUCTION

Studies of the intermetallic compound Ni<sub>3</sub>Al have both scientific and technological significance. First of all, this nickel-rich aluminide has attractive properties for structural applications at elevated temperatures:<sup>1</sup> since the flow stress increases with increasing temperature to a maximum value which occurs in the temperature region between 600 and 800°C, Ni<sub>3</sub>Al is the most important strengthening phase of the Ni-based superalloys. Further, the density of Ni<sub>3</sub>Al is significantly lower than that of the other Ni-based superalloys, and Ni<sub>3</sub>Al alloys have excellent oxidation resistance. However, it has been widely recognized that, unlike its single-crystal form, polycrystalline Ni<sub>3</sub>Al undergoes brittle intergranular fracture; hence, to be generally useful as an engineering material, one has to overcome its severe embrittlement and improve its ductility. Considerable effort has been made to increase the grain-boundary cohesion<sup>2</sup> and simultaneously to keep the high-symmetry cubic crystal structure upon addition of ternary elements. Therefore, theoretical understanding of the crystal stability of Ni<sub>3</sub>Al may have important significance in developing materials with sufficient ductility.

Secondly, experimental and theoretical data has accumulated for Ni<sub>3</sub>Al as a weak ferromagnetic system for the past two decades (for instance, measurement of magnetic properties,<sup>3</sup> low-temperature specific heat,<sup>4</sup> neutron scattering,<sup>5</sup> optical constants,<sup>6</sup> de Haas-van Alphen

effect,<sup>7</sup> and energy-band calculations,<sup>8-11</sup> etc.). de Boer *et al.*<sup>3</sup> concluded that the ordered,  $L_{12}$ -structured Ni<sub>3</sub>Al belongs to a weak itinerant-electron ferromagnetic regime with  $T_c = 41$  K. The temperature dependence of the magnetization, resistivity, magnetoresistance,<sup>12</sup> etc. showed that the effect of spin fluctuations is significant in Ni<sub>3</sub>Al. However, controversy has remained concerning the density of states at the Fermi level and the magnetic moment of Ni<sub>3</sub>Al. The observed saturation magnetic moment  $m$  is  $0.24\mu_B$  per cell;<sup>3</sup> on the other hand, the calculated values vary and range from nearly 0 to  $0.6\mu_B$  per cell. Hankenbracht and Kübler<sup>8</sup> (HK) obtained  $m = 0.093\mu_B$  per cell, whereas Buiting *et al.*<sup>9</sup> found  $m \simeq 0.203\mu_B$  per cell, and Maclin *et al.*<sup>10</sup>  $0.60\mu_B$  per cell—all at the calculated equilibrium lattice constant. However, at the experimental lattice constant (3.568 Å), HK (Ref. 8) obtained  $m = 0.23\mu_B$  per cell, Buiting *et al.*<sup>9</sup>  $0.02\mu_B$  per cell, and, more recently, Min *et al.*<sup>11</sup>  $0.44\mu_B$  per cell. Further, only a few papers have addressed the question of the structural stability of Ni<sub>3</sub>Al based on electronic-structure calculations.<sup>8,13</sup>

In this paper we focus on the structural stability of Ni<sub>3</sub>Al in three different crystal structures—cubic  $L_{12}$ , tetragonal  $DO_{22}$ , and hexagonal  $DO_{19}$  (cf. Fig. 1)—for which the total energy was calculated by means of the all-electron semirelativistic linear muffin-tin orbitals (LMTO) method based on the Hohenberg-Kohn-Sham local-density-functional approach.<sup>14</sup> We find that of these three different structures, the (weakly ferromagnet-

ic)  $L1_2$  structure is the most stable and is characterized by a low density of states at the Fermi level [4.49 states/eV f.u. (f.u.=formula unit) in its ferromagnetic state]. Additionally, the spin-polarized results for the  $L1_2$  phase are found to be consistent with Ref. 11, i.e., the ferromagnetic state is slightly lower in energy than that in the paramagnetic state. We find that the exchange energy gained by inducing a magnetic moment in Ni<sub>3</sub>Al is much smaller than the increase in band energy due to the structural transition into the  $D0_{22}$  (or  $D0_{19}$ ) phase. As in the case of Ni<sub>3</sub>V,<sup>15</sup> atomic ordering (or crystal structure) in Ni<sub>3</sub>Al dominates over the magnetism.

## II. COMPUTATIONAL DETAILS

Ni<sub>3</sub>Al crystallizes in the cubic  $L1_2$ -type structure with Al atoms occupying the cubic corners and Ni atoms at the face-center positions. However, to study the structural stability, we calculated the total energy for the three different structures, i.e., cubic  $L1_2$ , tetragonal  $D0_{22}$ , and hexagonal  $D0_{19}$  (cf. Fig. 1). Concerning ideal atomic ordering, all three are close-packed structures and each atom has the same coordination number of 12 atoms as first-nearest neighbors; in particular, there are no direct Al and Al-atom contacts, i.e., 12 Ni atoms surround each

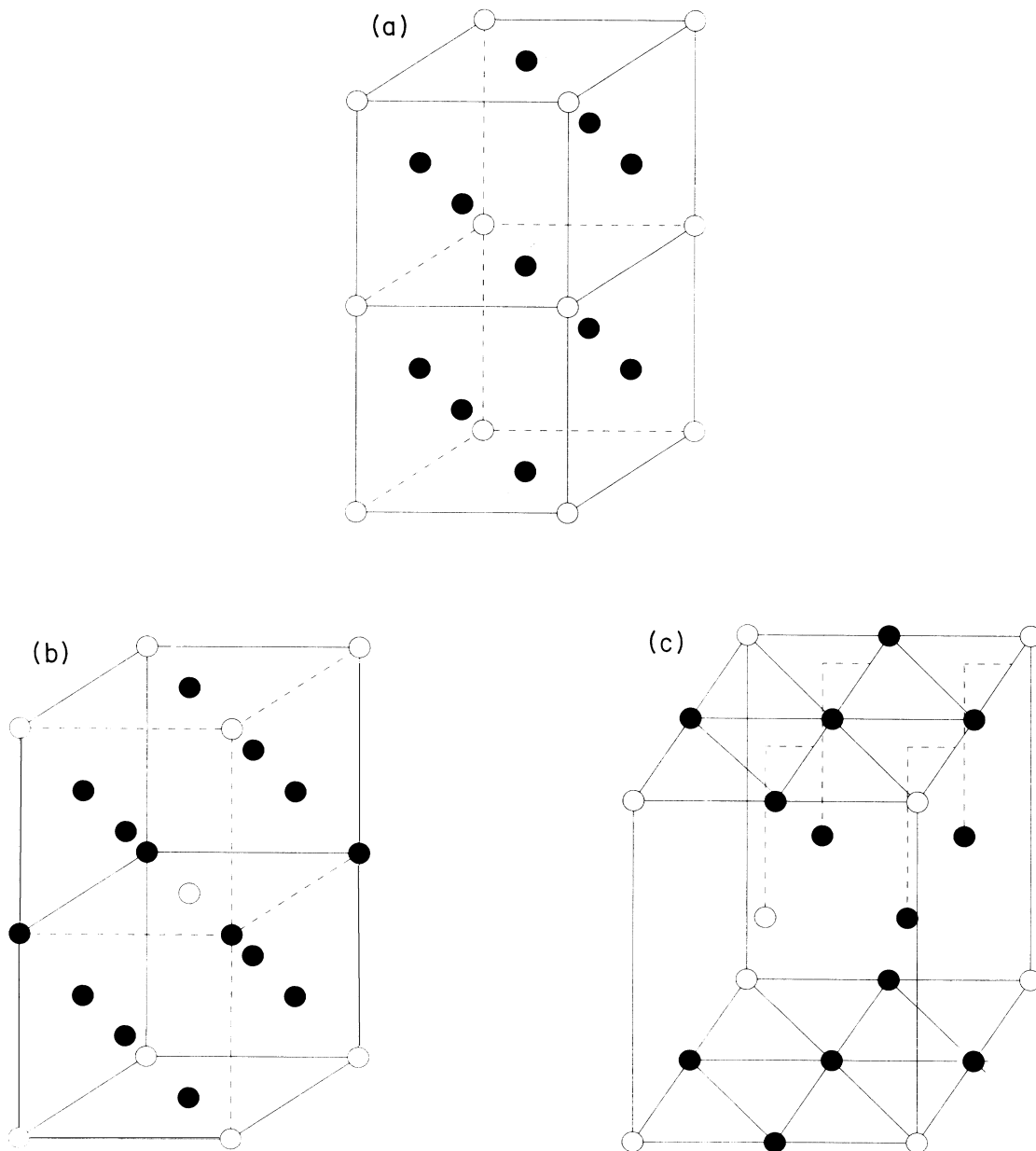


FIG. 1. Three different crystal structures—(a)  $L1_2$ , (b)  $D0_{22}$ , and (c)  $D0_{19}$ —of Ni<sub>3</sub>Al. The double cell for the  $L1_2$  structure is shown for easy comparison with the  $D0_{22}$  structure.

Al atom, and four Al atoms plus eight Ni atoms surround each Ni atom. Therefore, the total-energy difference due to the different crystal structure merely reflects the effect of atomic order to higher order. Clearly, we expect that the different atomic configurations will result in different Ni *d*—Ni *d* and Ni *d*—Al *p* bonding (hence, different phase stability). In fact, as will be seen later, the energetics mainly depend upon atomic ordering (i.e., on the Ni *d*—Ni *d* and Ni *d*—Al *p* bonding), and the magnetism has far less significance on the phase stability in Ni<sub>3</sub>Al. In the calculation it is reasonable to assume that both Ni and Al atoms have the same Wigner-Seitz-sphere radii, because the metallic radius of Ni (1.3 Å) is close to that of Al (1.4 Å). The *c/a* ratio was retained constant at 2.036 for the *DO*<sub>22</sub> structure [which is the observed *c/a* value of the tetragonal *DO*<sub>22</sub> phase of Ni<sub>3</sub>V (Ref. 16) and 0.816 for *DO*<sub>19</sub> (which is the ideal value of the close-packed structure).

Both paramagnetic and spin-polarized calculations were performed using the all-electron self-consistent local-density total-energy approach implemented by the LMTO method of Anderson. The fully relativistic core states were recalculated at every iteration, and the valence electrons were treated in a semirelativistic way, i.e., the spin-orbit interaction was not taken into account. The Hedin-Lundqvist and von Barth-Hedin formalism<sup>17</sup> for the exchange and correlation potential was adopted.

For understanding the effects of spin-orbit coupling on the magnetism, the spin-orbit interaction, *L*·*S*, is included in the semirelativistic Hamiltonian in a perturbative way. For conceptual simplicity, we assume that spin is still a good quantum number (approximately) even with the spin-orbit interaction included. The spin-up and -down potentials are used for the construction of diagonal parts of the spin-orbit Hamiltonian, whereas the average of spin-up and -down potentials is used for the off-diagonal parts. In this way we treat the spin-exchange interaction and spin-orbit interaction simultaneously on the same footing.

In order to determine the stability of the different structures, we calculated the total energy of each structure at a series of different lattice constants chosen close to the minimum total energy, using 60 *k* points within an irreducible wedge (for instance,  $\frac{1}{48}$  for the *L*<sub>12</sub> structure) of the Brillouin zone (IBZ). In principle, for judging the structural stability an accurate value of the total energy is required. However, it has been known<sup>18</sup> that the total energy depends on the sampling number of *k* points within the irreducible wedge of the Brillouin zone (IBZ). Since the total energy has a lower value calculated with the larger number of *k* points, an accurate value has to be obtained by extrapolating the value of the total energy obtained from several different (a finite number of) *k* points to the limit of an infinite number of *k* points within the IBZ. As in the case of Ni<sub>3</sub>V,<sup>15</sup> the use of 60 *k* points within the IBZ is sufficient to judge structural stability, because the total-energy difference due to the different structures is nearly 1 order of magnitude larger than the error due to the different (finite) number of *k* points used. However, for obtaining the formation energy, we adopt the total energy after extrapolating to an infinite number

of *k* points. The formation energy is defined as the energy difference between the compound and the weighted sum of the metallic constituents. Subsequently, for obtaining the magnetic moment of the cubic *L*<sub>12</sub>-structure Ni<sub>3</sub>Al, we adopted the use of 326 *k* points within the  $\frac{1}{48}$  wedge of the IBZ. Self-consistency of the charge density was assumed when the deviation between input and output potentials was less than 1 mRy. The parabolic fitting procedure was employed to obtain the bulk modulus.

### III. RESULTS AND DISCUSSIONS

The total energy ( $E_{\text{tot}}$ ) calculated as a function of the Wigner-Seitz radius ( $r_{\text{WS}}$ ) in the cubic *L*<sub>12</sub>, tetragonal *DO*<sub>22</sub>, and hexagonal *DO*<sub>19</sub> structures is shown in Fig. 2. As seen, for the entire region of the volume variation, the total energy of Ni<sub>3</sub>Al in the *L*<sub>12</sub> structure is always 15–20 mRy/f.u. lower than that in the *DO*<sub>22</sub> or *DO*<sub>19</sub> structures, and the total-energy difference between the latter two structures is only about 2 mRy/f.u. This indicates clearly that, in agreement with observation, the cubic *L*<sub>12</sub> phase of Ni<sub>3</sub>Al is the most stable phase among these three different phases.

The calculated cohesive properties (including the equilibrium lattice constant, Wigner-Seitz radius, bulk modulus, and formation energy, etc.) obtained from the total energy are listed in Table I. In general, the agreement between the calculated and observed results must be considered quite good: The calculated formation energy (44.8 kcal/mol) for the *L*<sub>12</sub> phase is in fairly good agreement with experiment [36.6 kcal/mol (Ref. 19) and 37.5 kcal/mol (Ref. 20)]. The calculated equilibrium Wigner-Seitz radii and bulk moduli for the different structures

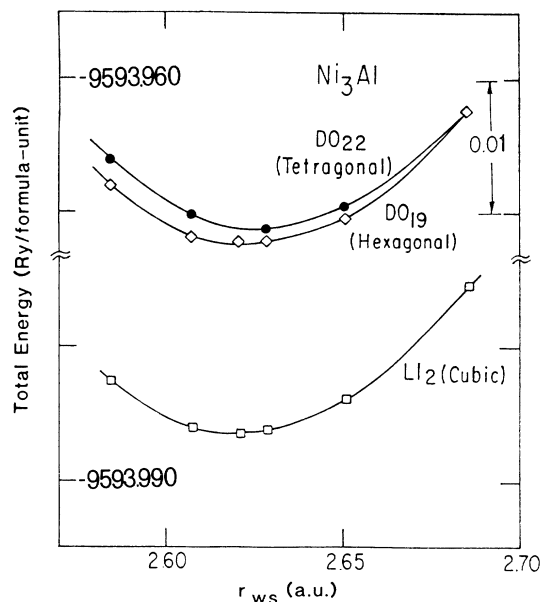


FIG. 2. Total energy as a function of the Wigner-Seitz radius and its structure dependence for Ni<sub>3</sub>Al (in paramagnetic states) using 60 *k* points within the IBZ; squares, solid circles, and diamonds indicate the *L*<sub>12</sub>, *DO*<sub>22</sub>, and *DO*<sub>19</sub> structures, respectively.

TABLE I. Equilibrium lattice constants ( $a$  and  $c$ ), Wigner-Seitz-sphere radii ( $r_{\text{WS}}^0$ ), bulk moduli ( $B$ ), and formation energies ( $E$ ) for the three different structures ( $L1_2$ ,  $D0_{22}$ , and  $D0_{19}$ ) of Ni<sub>3</sub>Al compared with available experimental data.

Crystal structure	$a$ (Å)		$c$ (Å) (calc.)	$r_{\text{WS}}^0$ (a.u.)	$B$ (Mbar)		$E$ (kcal/mol)	
	Calc.	Expt.			Calc.	Expt.	Calc.	Expt.
$L1_2$	3.55	3.56 <sup>b</sup>	7.20	2.622	2.0–2.1	2.4 <sup>d</sup>	44.8	36.6 <sup>e</sup>
	3.53 <sup>a</sup>				2.1 <sup>a</sup>			37.5 <sup>b</sup>
					2.12 <sup>c</sup>			
$D0_{22}$	3.54		7.20	2.629	2.0		40.4	
$D0_{19}$	5.02		4.10	2.621	1.9		41.1	

<sup>a</sup>Reference 8.

<sup>b</sup>Reference 20.

<sup>c</sup>Reference 11.

<sup>d</sup>Reference 21.

<sup>e</sup>Reference 19.

are the same within the numerical precision; the calculated equilibrium Wigner-Seitz radius (or, equivalently, the lattice constant 3.55 Å) for the  $L1_2$  phase is in good agreement with the observed value, 3.56 Å,<sup>20</sup> or 3.568 Å,<sup>8</sup> and the bulk modulus (2.0–2.1 Mbar) agrees well with experiment (2.4 Mbar),<sup>21</sup> and with the results of other calculations<sup>8,11</sup> (cf. Table I).

We next considered the effect of magnetism on the total energy. Table II lists the dependence of the total energy versus lattice constant for the cubic  $L1_2$ -structured Ni<sub>3</sub>Al in the paramagnetic and spin-polarized states. As seen in Table I, the total energy of the ferromagnetic state is only 0.2–0.5 mRy/f.u. lower than that of the paramagnetic state. This result is consistent with the full-potential linear augmented-plane-wave (FLAPW) results of Ref. 11 that the ferromagnetic state is slightly lower in energy ( $\sim 1$  mRy/f.u.) than the paramagnetic state. In the  $D0_{19}$  case, we have found a similar decrease (by  $\sim 0.3$  mRy/f.u.) of the total energy for the ferromagnetic state compared to the paramagnetic state (cf. Table III). Thus, the ferromagnetic state is also found for this structure. These results demonstrate that, as found in the case of Ni<sub>3</sub>V,<sup>15</sup> the energy gain in Ni<sub>3</sub>Al caused by magnetic effects is nearly 1 order of magnitude smaller than that due to the structural difference (cf. Table III). Therefore, we can conclude that (i) cubic  $L1_2$ -structured Ni<sub>3</sub>Al (in the weak ferromagnetic state) is the most stable phase, and (ii) the structure difference or atomic ordering dominates over the magnetism in the sense that the

TABLE II. Dependence of the total energy on the lattice constant for  $L1_2$ -structured Ni<sub>3</sub>Al using 60  $\mathbf{k}$  points within the  $\frac{1}{48}$  IBZ.

$a$ (Å)	$r_{\text{WS}}$ (a.u.)	$E_{\text{tot}}$ (Ry/f.u.)	
		Paramagn.	Ferromagn.
3.50	2.5847	–9593.9825	–9593.9827
3.53	2.6080	–9593.9859	–9593.9861
3.55	2.6217	–9593.9863	–9593.9866
3.56	2.6291	–9593.9861	–9593.9865
3.59	2.6518	–9593.9837	–9593.9842

magnetism plays no crucial role on the phase stability.

The total and partial (i.e., angular-momentum-projected) density of states at the Fermi level and the partial charge occupancies of ferromagnetic Ni<sub>3</sub>Al are listed in Table IV. For comparison, the results of Ref. 11 are also listed. As seen from Table IV, the main contribution for the magnetic moment of Ni<sub>3</sub>Al comes from that of the Ni  $d$  electrons and appears irrelevant to the method used; in the present results uncompensated Al  $p$  electrons are polarized slightly negatively, which is also seen in the results of Ref. 11 in the interstitial region. The magnetic moment of  $0.71\mu_B$  per cell is close to the moment of  $0.60\mu_B$  per cell obtained by Maclin *et al.*<sup>10</sup> also using the LMTO band method, but is comparatively larger than that ( $0.44\mu_B$  per cell) given by the FLAPW calculation, and much larger than those of (HK),<sup>8</sup> Buiting *et al.*,<sup>9</sup> and the experimental value of  $0.24\mu_B$  per cell.<sup>3</sup> Our calculated exchange-energy splitting between spin-up and -down bands near the Fermi level is rather uniform over Brillouin zone, about 19 mRy. Since it is larger than that of

TABLE III. Total energy and total density of states at  $E_F$  for the three different structures ( $L1_2$ ,  $D0_{22}$ , and  $D0_{19}$ ) of Ni<sub>3</sub>Al; for the  $L1_2$  structure paramagn. and ferromagn. represent the paramagnetic and ferromagnetic states, respectively, and  $E_{\text{tot}}(\infty)$  represents the extrapolated value of the total energy corresponding to an infinite number of  $\mathbf{k}$  points within the IBZ.

Crystal structure	$E_{\text{tot}}(\infty)$ (Ry/f.u.)	$N(E_F)$ (states/eV f.u.)		
		Calc.	Expt.	
$L1_2$	paramagn.	–9593.9876	7.40	11.03 <sup>b</sup>
	ferromagn.	–9593.988	4.49	12.84 <sup>c</sup>
			4.35 <sup>a</sup>	
$D0_{22}$	–9593.9738	4.91		
$D0_{19}$	paramagn.	–9593.9753	7.33	
	ferromagn.	–9593.976	5.27	

<sup>a</sup>Reference 9.

<sup>b</sup>Reference 4.

<sup>c</sup>Reference 23.

TABLE IV. Partial DOS at  $E_F$ ,  $N_l(E_F)$  (in states/Ry f.u.) and partial charge occupancies (in electrons per atom) of ferromagnetic  $\text{Ni}_3\text{Al}$ . Present results and those of Ref. 11 are calculated at the theoretical and experimental equilibrium lattice constants, respectively.

		Spin	Ni $s$	Ni $p$	Ni $d$	Ni $f$	Al $s$	Al $p$	Al $d$	Al $f$	Interstitial region	Total
$N_l(E_F)$	Present	$\uparrow$	0.08	0.50	5.35		0.30	0.28	0.20			18.75
		$\downarrow$	0.12	0.65	13.10		0.35	0.23	0.30			42.49
	Ref. 11	$\uparrow$	0.08	0.24	7.65	0.01	0.26	0.15	0.09	0.01	2.00	24.45
		$\downarrow$	0.08	0.27	14.62	0.01	0.24	0.10	0.10	0.01	2.49	45.39
$n_l$	Present	$\uparrow$	0.34	0.41	4.45		0.45	0.58	0.19			16.82
		$\downarrow$	0.34	0.42	4.22		0.45	0.60	0.19			16.18
	Ref. 11	$\uparrow$	0.16	0.15	4.10	0.01	0.25	0.26	0.06	0.01	2.88	16.72
		$\downarrow$	0.17	0.15	3.95	0.01	0.25	0.26	0.06	0.01	2.90	16.28

the FLAPW calculation<sup>11</sup> (12 mRy), it gives rise to a larger magnetic moment.

In addition, we studied the dependence of the magnetic moment on pressure by calculating the magnetic moment at different lattice constants for the  $L1_2$  phase. In contrast to<sup>22</sup> Ref. 9, our calculated magnetic moment increases rather linearly from  $0.61\mu_B$  per cell to  $0.76\mu_B$  per cell as the lattice constant increases from 3.50 to 3.59 Å. The change of electron distributions (and the total number of electrons) for each spin is insensitive to the variation of lattice constant. Once one adopt the experimental value (2.4 Mbar) of the bulk modulus of  $\text{Ni}_3\text{Al}$ , then one estimates the pressure dependence of the magnetic moment,  $\Delta\sigma/\Delta p = -0.2\mu_B/\text{Mbar atom}$ . Note that this is about half of the experimental value<sup>23</sup> ( $-0.408\mu_B/\text{Mbar atom}$ ). The quantitative discrepancy, however, does not have to be taken literally, since the value is very sensitive to many parameters in both experiment and calculation. For example, the value depends on the range of lattice constant that is measured or calculated. It is expected that the value would be large near the critical pressure  $P_c$  where the magnetization disappears and becomes small as the magnetic moment saturates at the expanded lattice constant.

The difference between our result and experiment is considerably reduced by taking spin-orbit coupling into account. The spin-orbit interaction does not make any difference in the angular-momentum charge decomposition, but rearranges the partial occupancies of spin-up and -down electrons in the Ni  $d$  band. The energy gain by including the spin-orbit interaction is 1–2 mRy. More significantly, the exchange splitting is reduced by  $\sim 40\%$ . This large reduction reflects a lowering of the density of states at the Fermi level due to the spin-orbit splitting. Remarkably, the reduced splitting is about 11 mRy, which is close to the FLAPW value without spin-orbit coupling and leads to a similar (now reduced by  $\sim 40\%$ ) spin magnetic moment,  $0.42\mu_B$ . There is also an orbital contribution to the magnetic moment which originates mostly from the Ni  $d$  electrons ( $0.04\mu_B$ ), which makes the total magnetic moment per cell  $0.46\mu_B$ , which is still 2 times larger than experiment.

(Interestingly, if we assume this reduction due to spin-orbit coupling to occur uniformly if included in the

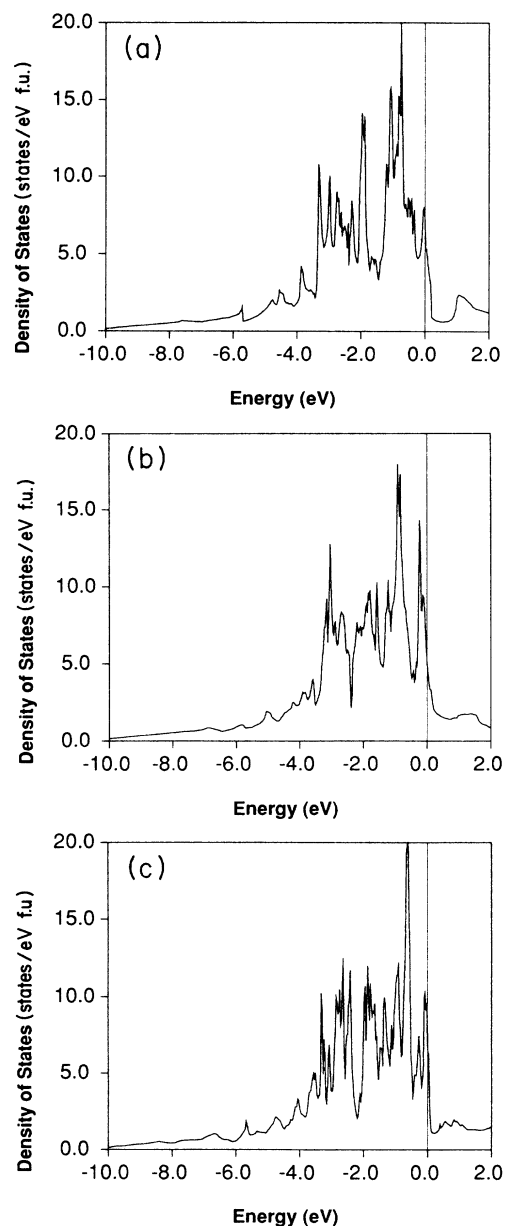


FIG. 3. Total density of states for  $\text{Ni}_3\text{Al}$  in (a)  $L1_2$ , (b)  $D0_{22}$ , and (c)  $D0_{19}$ . The Fermi level is taken as zero energy.

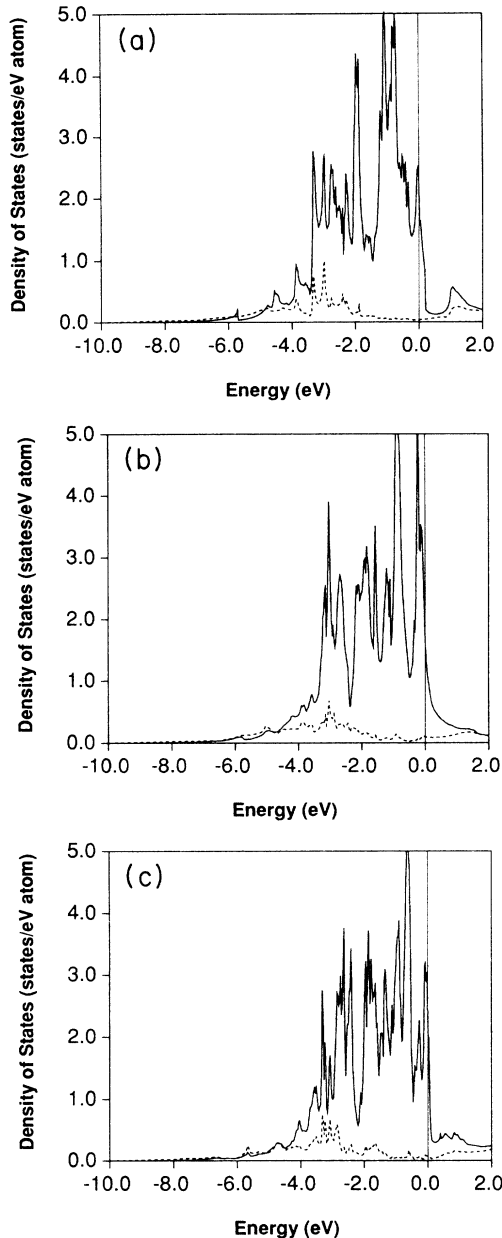


FIG. 4. Partial (projected by angular momentum and site) density of states for Ni<sub>3</sub>Al in (a)  $L1_2$ , (b)  $D0_{22}$ , and (c)  $D0_{19}$ . Solid and dashed lines represent Ni  $d$  and Al  $p$  contributions, respectively. The Fermi level is taken as zero energy.

FLAPW calculations, the exchange splitting becomes 7 mRy and the magnetic moment now becomes  $0.23\mu_B$ , which is very close to the experimental value.)

In order to understand the phase stability of Ni<sub>3</sub>Al, we inspect the paramagnetic density of states (DOS) shown in Fig. 3. It is seen that the Fermi level of Ni<sub>3</sub>Al in both the  $L1_2$  and  $D0_{19}$  structures lies close to one of the DOS peaks; therefore, the DOS at the Fermi level,  $N(E_F)$ , for Ni<sub>3</sub>Al in the  $L1_2$  (or  $D0_{19}$ ) structure has a fairly high value (7.40 or 7.44 states/eV f.u.) (cf. Table III). It is interesting to note that Ni<sub>3</sub>Al in its  $D0_{22}$  structure has the lowest  $N(E_F)$  (4.91 states/eV f.u.) of the three structures

in the paramagnetic state. However, the  $N(E_F)$  of the spin-polarized calculation for the cubic ( $L1_2$ ) phase is only 4.49 states/eV f.u., i.e.,  $N(E_F)$  in the ferromagnetic state is reduced to about half of that in the paramagnetic state. [This reduction is much larger than that found in the FLAPW calculations reported in Ref. 11—again indicating the sensitivity of  $N(E_F)$ .] The high-DOS peak near  $E_F$  in the paramagnetic  $L1_2$  phase is exchange split apart in the spin-polarized case, and thus the spin-up DOS is nearly filled up; this results in a small density of states. Taken together, the results clearly demonstrate that a correlation between stability and  $N(E_F)$  exists in this intermetallic compound, such that the energetically favorable atomic arrangement has a low DOS at the Fermi level.<sup>15,24</sup>

It is well known that the cohesive energy of the transition metal arises from the strong bonding on the  $d$  valence electrons.<sup>25</sup> According to HK,<sup>8</sup> the  $d$ -band energy difference approximately reproduced the trend in the heats of formation for Ni<sub>3</sub>Al and Ni-Al. In the sense of the Ni  $d$  band dominating the cohesion of the Ni-rich compounds, Ni<sub>3</sub>Al in the  $L1_2$  structure is energetically favored over the  $D0_{22}$  structure, because in all three structures, as mentioned before, each atom has same first-nearest-neighbor environment, but, if we inspect the Ni  $d$ —Ni  $d$  bonding up to the second-nearest neighbor, we find that there are two more Ni  $d$ —Ni  $d$  bonds in the  $L1_2$  (or  $D0_{19}$ ) structure as compared to the  $D0_{22}$  structure.

Furthermore, it can be seen clearly that another characteristic feature of the density of states in Ni<sub>3</sub>Al is the hybridization between Ni  $d$  and Al  $p$  states (cf. Fig. 4), which depends strongly on the atomic ordering (or crystal structure). Note that the most significant feature of the electronic structure for Ni<sub>3</sub>Al in the  $L1_2$  phase is a deep valley located at about 0.5 eV above  $E_F$ , which separates the  $p$ - $d$  bonding and antibonding states. As shown in Fig. 4, a sharp Al  $p$  bonding (antibonding) peak is located in the region near  $-3$  eV (1 eV) for the  $L1_2$  structure. On the other hand, this feature nearly disappears in the other two structures with a smooth and much more diffuse Al  $p$  structure located nearly in the same energy region. This obviously indicates that the hybridization between Ni  $d$  and Al  $p$  states in the  $L1_2$  structure is much stronger than that in other two structures. In other words, besides the Ni  $d$  and Ni  $d$  bonding, the strong hybridization between Ni  $d$  and Al  $p$  states tends to favor the cubic  $L1_2$  structure over the hexagonal  $D0_{19}$  and tetragonal  $D0_{22}$  structures.

Note that if only up to second-nearest-neighbor Ni  $d$ —Al  $p$  hybridization is taken into account, the  $D0_{22}$  crystal structure is favored over the  $L1_2$  structure because each Ni atom has two Al atoms and four Ni atoms as second-nearest neighbors in the  $D0_{22}$  structure, and there are no Al atoms as second-nearest neighbors in the  $L1_2$  structure. Since Ni<sub>3</sub>Al in the  $L1_2$  structure is energetically favored over the  $D0_{22}$  structure, it is clearly not sufficient to judge the structural stability by considering only first- and second-nearest-neighbor couplings; in other words, higher-order nearest-neighbor interactions be-

tween Ni  $d$  and Al  $p$  states in Ni<sub>3</sub>Al may play a significant role in the determination of its structural stability. Finally, it should be pointed out that the bonding nature of Ni<sub>3</sub>Al is apparently different from the case of<sup>15</sup> Ni<sub>3</sub>V, for which the second-nearest-neighbor coupling between the Ni  $d$  and V  $d$  states was found to be responsible for its structural stability. This structural-stability difference between Ni<sub>3</sub>Al and Ni<sub>3</sub>V can be traced back to the difference between the Al  $p$  and the V  $d$  states, since the Al  $p$  states in Ni<sub>3</sub>Al have a relatively long-range tail compared with V  $d$  states in Ni<sub>3</sub>V.

#### ACKNOWLEDGMENTS

This work was supported by the U.S. Air Force Office of Scientific Research (AFOSR) under Grant No. 85-0358, and by a grant of computer time at the Wright-Patterson Air Force Base Supercomputing Center. One of us (B.I.M.) acknowledges financial support from the Korean Science and Engineering Foundation and from POSTECH. Helpful discussions with J. I. Lee and H. J. F. Jansen are greatly appreciated.

- <sup>1</sup>*Intermetallic Compounds*, edited by J. H. Westbrook (Wiley, New York, 1967).
- <sup>2</sup>K. Aoki and O. Izumi, *Nippon Kinzoku Gakkaishi* **43**, 1190 (1979); C. T. Liu and C. C. Koch, in *Proceedings of a Public Workshop on Trends in Critical Materials Requirements for Steels of the Future: Conservation and Substitution Technology for Chromium* (U.S. GPO, Washington, D.C., 1983).
- <sup>3</sup>F. R. de Boer, C. J. Schinkel, J. Biesterbos, and S. Proost, *J. Appl. Phys.* **40**, 1049 (1969); N. Buis, Ph.D. thesis, University of Amsterdam, 1979.
- <sup>4</sup>W. de Dood and P. F. de Châtel, *J. Phys. F* **3**, 1039 (1973); S. K. Dhar and K. A. Gschneidner, *Phys. Rev. B* **39**, 7453 (1989).
- <sup>5</sup>N. R. Bernhoeft, G. G. Lonzarich, P. W. Mitchell, and D. McPaul, *Phys. Rev. B* **28**, 422 (1983).
- <sup>6</sup>P. A. M. van der Heide, J. J. M. Buiting, L. M. ten Dam, L. W. M. Schreurs, R. A. de Groot, and A. R. de Vroomen, *J. Phys. F* **15**, 1195 (1985).
- <sup>7</sup>G. G. Lonzarich, T. I. Sigfusson, J. J. M. Buiting, J. Kübler, and F. M. Mueller, *J. Appl. Phys.* **53**, 3 (1982).
- <sup>8</sup>D. Hackenbracht and J. Kübler, *J. Phys. F* **10**, 427 (1980).
- <sup>9</sup>J. J. M. Buiting, J. Kübler, and F. M. Mueller, *J. Phys. F* **13**, L179 (1983).
- <sup>10</sup>A. P. Maclin, G. M. Stocks, and W. M. Temmerman, in *High Temperature Alloys*, Bethesda, 1984, edited by J. O. Stigler (Metallurgical Society of AIME, Bethesda, MD, 1984).
- <sup>11</sup>B. I. Min, A. J. Freeman, and H. J. F. Jansen, *Phys. Rev. B* **37**, 6757 (1988). A preliminary report of our LMTO results is included in this paper.
- <sup>12</sup>H. Sasakura, K. Suzuki, and Y. Masada, *J. Phys. Soc. Jpn.* **53**, 352 (1984); **53**, 754 (1984); K. Suzuki and Y. Masada, *ibid.* **54**, 326 (1984); **54**, 630 (1985).
- <sup>13</sup>G. M. Stocks, D. M. Nicholson, F. J. Pinski, W. H. Bulter, P. Sterne, W. M. Temmerman, B. L. Gyorffy, D. D. Johnson, A. Gonis, X.-G. Zhang, and P. E. A. Turchi, in *High Temperature Ordered Intermetallic Alloys II*, Mater. Res. Soc. Symp. Proc. No. 81, edited by N. S. Stoloff, C. C. Koch, C. T. Liu, and O. Izumi (MRS, Pittsburgh, 1987), p. 15.
- <sup>14</sup>O. K. Andersen, *Phys. Rev. B* **12**, 3060 (1975).
- <sup>15</sup>J.-h. Xu, T. Oguchi, and A. J. Freeman, *Phys. Rev. B* **36**, 4186 (1987).
- <sup>16</sup>For our study of Ni<sub>3</sub>(Al,V), we took the  $c/a$  ratio of Ni<sub>3</sub>Al to be the same as the experimental value of  $c/a$  for Ni<sub>3</sub>V.
- <sup>17</sup>L. Hedin and B. Lundqvist, *J. Phys. C* **4**, 2064 (1971); U. von Barth and L. Hedin, *ibid.* **5**, 1629 (1972).
- <sup>18</sup>H. J. F. Jansen and A. J. Freeman, *Phys. Rev. B* **30**, 561 (1984).
- <sup>19</sup>O. Kubaschewski, E. LL. Evans, and C. B. Alcock, *Metallurgical Thermochemistry*, 4th ed. (Pergamon, Oxford, 1979).
- <sup>20</sup>*Smirhells Metals Reference Book*, 6th ed., edited by E. A. Brandes (Butterworths, London, 1983).
- <sup>21</sup>J. J. M. Franse, M. Rosen, and E. P. Wohlfarth, *Physica B+C (Amsterdam)* **86-88B**, 317 (1977).
- <sup>22</sup>In Ref. 9 they found that the magnetic moments increased dramatically from  $\sim 0.02\mu_B$  per cell to  $0.203\mu_B$  per cell as the lattice constant varied from 3.568 to 3.583 Å.
- <sup>23</sup>N. Buis, J. J. M. Franse, and P. E. Brommer, *Physica B+C (Amsterdam)* **106B**, 1 (1981).
- <sup>24</sup>V. L. Moruzzi, P. Oelhafen, and A. R. Williams, *Phys. Rev. B* **27**, 7194 (1983).
- <sup>25</sup>J. Friedel, in *The Physics of Metals*, edited by J. M. Ziman (Cambridge University Press, London, 1969), Chap. 8; D. G. Pettifor, *Phys. Rev. Lett.* **42**, 846 (1979).